Chemical Engineering Journal 509 (2025) 161303

Contents lists available at ScienceDirect

Chemical Engineering Journal

journal homepage: www.elsevier.com/locate/cej

Near-infrared light-triggered in situ self-assembly nanomedicine for treating antibiotic-resistant bacterial infection

Yu Zhang [a,b], Chunhua Ren [c,*], Huayang Liu [b], Jingyi Duan [c], Mengyao Wang [a], Ziao Zhou [b], Jinyou Duan [a,*], Huaimin Wang [b,*], Xiaoli Zhang [a,*]

[a] College of Chemistry & Pharmacy, Northwest A&F University, Yangling, Shaanxi 712100, China
[b] Department of Chemistry, School of Science, Westlake University, No. 600 Yungu Road, Hangzhou 310030 Zhejiang Province, China
[c] Institute of Radiation Medicine, Chinese Academy of Medical Sciences & Peking Union Medical College, Tianjin 300192, China

ARTICLE INFO

Keywords:
In situ self-assembly
Peptide-based nanomedicine
Antibiotic resistance
Bacterial infection
Biofilm removal

ABSTRACT

Antibiotic-resistant bacterial infections are increasing at an alarming rate, posing a significant threat to global health and highlighting the urgent need for innovative therapeutic strategies. Herein, we developed a near-infrared (NIR) photoactivatable amphiphilic precursor molecule of peptide-vancomycin conjugate (PFTV), which could in situ self-assemble into a nanogermicidal agent on bacterial surfaces upon exposure to NIR light. This approach aimed to effectively treat infections caused by vancomycin-resistant Enterococcus (VRE). Our findings indicated that the in situ self-assembly of PFTV triggered by NIR light demonstrated superior antiplanktonic activity compared to free vancomycin, with the minimum inhibitory concentration reduced by two orders of magnitude. Additionally, this strategy enhanced PFTV penetration and removal of VRE biofilms, achieving a bacterial killing efficiency of 99%. Mechanistic studies revealed that the combination of PFTV and NIR light treatment eradicated antibiotic-resistant bacteria via two main actions: membrane perturbation and disruption of cellular homeostasis. Furthermore, the in situ self-assembly of PFTV upon NIR light irradiation demonstrated significant therapeutic efficacy in treating VRE-induced infections and accelerating wound healing in vivo by mitigating inflammation responses and promoting neovascularization. This work has reported an on-demand activated strategy to facilitate peptide-antibiotic conjugate in situ self-assembly into a multivalent nanoantibacterial agent, which could provide novel paradigm for targeted drug delivery and combating multidrug-resistant pathogens.

1. Introduction

Bacterial infections can lead to severe health issues and pose a significant threat to human life. Notably, infections caused by gram-positive bacteria can result in various serious conditions, including sepsis, bacteremia, pneumonia, osteomyelitis, and endocarditis [1–5]. Since Alexander Fleming discovered penicillin in 1928, a wide array of antibiotics has been utilized in clinical practice, effectively treating infections and helping control the spread of bacterial infectious diseases [6,7]. However, due to shifts in bacterial sensitivity and the misuse of antibiotics, the rise of multidrug-resistant (MDR) bacteria has become a major global public health concern, with the mortality rates associated with MDR infections increasing annually [8–10]. Despite ongoing efforts to modify existing antibiotic frameworks, this strategy is no longer sufficient to keep pace with the rapid emergence of new drug-resistant bacteria, necessitating the urgent development of alternative therapeutic approaches to combat antibiotic resistance [11–14].

Nanomaterial-based therapeutics have demonstrated significant potential in addressing antibiotic-resistant bacterial infections in recent years. The unique properties of nanomaterials, such as their high surface-to-volume ratios and multivalent interactions, enable them to bypass existing antibiotic resistance mechanisms, effectively targeting MDR planktonic bacteria and biofilm infections [15–17]. The bactericidal mechanisms of antibacterial nanomaterials primarily involve membrane destruction, catalytic killing, disruption of the electron transport chain, and cell division arrest [18–20]. Furthermore, nanomaterials can be engineered as advanced nanocarriers to deliver various therapeutic agents, including antibiotics, antibacterial peptides, and

* Corresponding authors.
E-mail addresses: renchunhua@irm-cams.ac.cn (C. Ren), jduan@nwsuaf.edu.cn (J. Duan), wanghuaimin@westlake.edu.cn (H. Wang), xiaoliflyhighly@163.com (X. Zhang).

https://doi.org/10.1016/j.cej.2025.161303
Received 25 January 2025; Received in revised form 3 March 2025; Accepted 5 March 2025
Available online 6 March 2025
1385-8947/

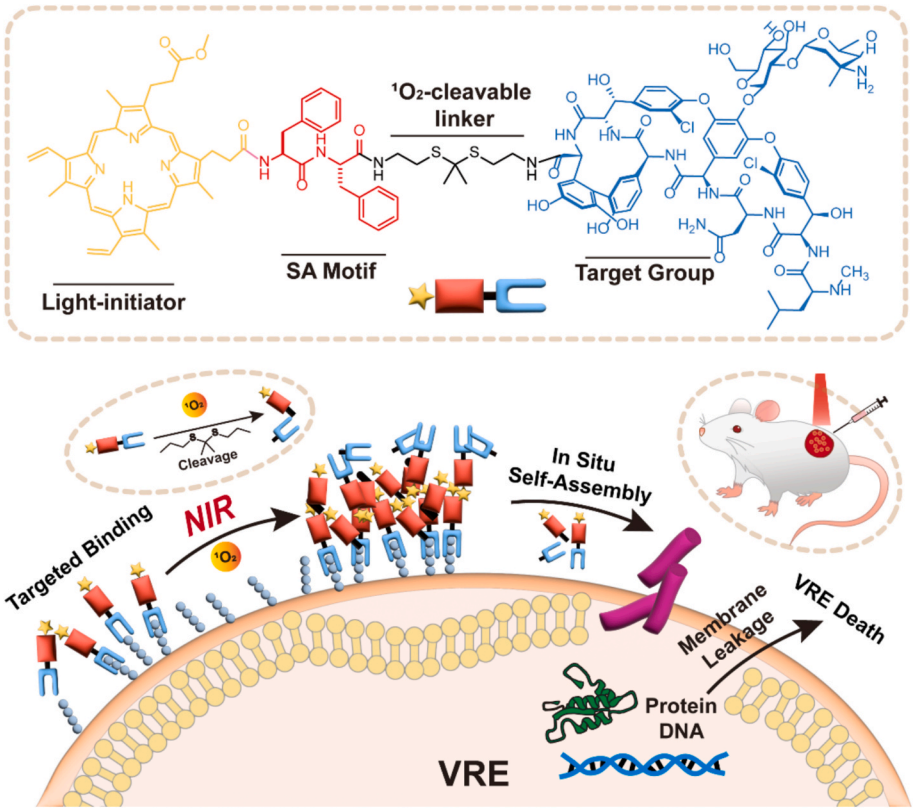

Scheme 1. Chemical structure of the PFTV and schematic illustration of NIR triggered in situ self-assembly of PFTV on the VRE surface. Upon NIR light exposure, the conjugated PpIX in PFTV generates $^1O_2$ and triggers cleavage of the involved thioketal linker. This process facilitates the in situ self-assembly (SA) of the resulted multi-components on the VRE surface forming multivalent nanoantibacterial agent, disrupting cell membrane integrity and ultimately leading to VRE death.

photosensitizers [21–23]. Despite the promising prospects of these nanomaterial-based therapeutics for treating MDR infection, several challenges persist in their practical application. These include inadequate quality control during large-scale production, low stability in various media, limited selectivity for targeted disease sites, and serious side effects on normal tissues [21,24,25]. As a result, there is an urgent need for innovative strategies to address the challenges associated with nanomaterial-based antibacterial therapies.

In situ self-assembly presents an effective strategy to address the aforementioned issues by seamlessly integrating the benefits of free drugs and nanodrugs. During the in situ self-assembly process, inactive precursors can be selectively transformed into functional nanoassemblies in response to endogenous or external stimuli at targeted infection sites [26,27]. Notably, many diseases exhibit substantial differences between diseased and normal cells, which has led to widespread research on utilizing endogenous stimuli—such as temperature, pH, and ionic strength—to activate designed molecules specifically at disease sites [28–30]. Meanwhile, the application of biocompatible external stimuli, such as light, ultrasound, and magnetic fields, for triggering in situ self-assembly has recently emerged as a promising strategy [31,32]. Light, in particular, offers advantages including good biosafety, low cost, and high spatiotemporal resolution, making it a focal point in various fields [33–35]. Among the different types of light, near-infrared (NIR) light is noteworthy for its superior tissue penetration depth and biocompatibility, which minimizes scattering and attenuation within living tissues [36]. Therefore, NIR has shown great promise for applications in in vivo imaging, cancer phototherapy, and other biomedical fields [37–40]. Although NIR has the risk of causing additional burns to the wound, it could be avoided by reducing the radiation intensity or shortening the exposure time [41]. However, the use of NIR to initiate in situ self-assembly for combating antibiotic-resistant bacteria remains relatively underexplored, especially in living systems.

Vancomycin, a glycopeptide antibiotic, effectively targets gram-positive bacteria by binding the D-Ala–D-Ala termini of uncrosslinked peptidoglycan precursors at the bacterial surface, thereby inhibiting cell wall synthesis [42,43]. Although vancomycin remains effective against certain drug-resistant strains, such as methicillin-resistant Staphylococcus aureus (MRSA), the mutation of D-Ala–D-Ala to D-Ala–D-Lac in various bacterial species compromises vancomycin binding specificity. This has contributed to the emergence of several resistant strains, including vancomycin-resistant S. aureus and vancomycin-resistant Enterococcus (VRE) [44]. Herein, we report the development of a NIR light–activatable in situ self-assembly of a peptide-vancomycin conjugate (PFTV) for the treatment of VRE-induced infections. As shown in Scheme 1, PFTV comprises a photosensitizer, protoporphyrin IX (PpIX), a self-assembly-promoting motif obtained from diphenylalanine (FF) [45,46], vancomycin, and a singlet oxygen ($^1O_2$)-cleavable linker of thioketal (TK). PFTV is designed to target the gram-positive bacterial cell wall and accumulate on the VRE membrane. Upon NIR irradiation, PpIX is activated to generate a high local concentration of $^1O_2$, which triggers cleavage of the TK linker and partial dissociation of the PpIX-FF (PFF) from vancomycin [47]. Subsequent to cleavage, under the influence of multiple noncovalent interactions, the resultant multi-components undergo in situ self-assembly, forming a multivalent nanoantibacterial agent on the bacterial surface. This assembly enhances the permeability of the VRE membrane and facilitates the leakage of cellular components, ultimately disrupting cellular homeostasis and inducing bacterial cell death. Given the advantages of on-demand activation provided by this approach, we propose that this study may serve as a foundational strategy for the development of in situ self-assembled nanoantibacterial agents aimed at overcoming resistant bacterial infections.

2. Materials and methods

2.1. Materials

All chemical reagents were reagent grade and were used as purchased without further notification. 2-Chlorotrityl Chloride Resin was purchased from Tianjin Nankai Hecheng Sci&Tech. Co. Ltd (Tianjin, China). HBTU and Fmoc-protected amino acid were obtained from GL Biochem (Shanghai, China). N, N-Diisopropylethylamine (DIPEA), Trifluoroacetic acid (TFA), Vancomycin hydrochloride (Van), Cystamine dihydrochloride, N, N'-dicyclohexyl carbodiimide (DCC), 4-Dimethylaminopyridine (DMAP) were bought from Aladdin (Shanghai, China). TK-NH_2 was bought from Kailiqi Biopharma Technology (Tianjin, China). Agar and N-Hydroxybenzotrizole (HOBT) were bought from Macklin (Shanghai, China). Protoporphyrin IX (PpIX) was bought from Adamas (Shanghai, China). HEK 293 T cell line was obtained from the American Type Culture Collection (ATCC). Vancomycin-resistant E. faecium (VREm, VanA) ATCC 51559, vancomycin-resistant E. faecalis (VREs, VanB) ATCC 51575, ATCC51299 were obtained from the ATCC. Brain Heart Infusion Broth (BHIB) was bought from Solarbio. DMEM, FBS, and Penicillin-Streptomycin solutions were purchased from Gibco. Crystal Violet Hydrate Solution, MTT, and Uranyl acetate dihydrate were bought from Sigma. Carbon-coated copper grids for TEM assays were obtained from Zhongjingkeyi Technology (Beijing, China). LIVE/DEAD BacLight Bacterial Viability Kit was bought from Thermo. 1,3-Diphenylisobenzofuran (DPBF) was bought from Heowns (Tianjin, China). BCA Protein Assay Kit was bought from Cwbio (Jiangsu, China). Male BALB/c mice (6–8 weeks, 20–24 g) were provided by Beijing Vital River Laboratory Animal Technology Co., Ltd. (Beijing, China).

2.2. Synthesis and characterization of compounds

We synthesized PpIX-FF and PpIX-GG by standard solid phase peptide synthesis (SPPS). The compounds of Van-TK, Van-S-S, PFTV, PGTV and PFSV were synthesized using organic synthesis methods, and the detailed experimental procedures can be found in the Supplementary Information.

2.3. Measurement of $^1O_2$ generation capacity in vitro

The singlet oxygen probe DPBF was used to assess $^1O_2$ generation. Briefly, 10 μM of each compound was mixed with 60 μM DPBF and irradiated at 635 nm, 500 mW/cm^2. DPBF absorbance at 422 nm was monitored every 10 s (Varioskan Lux, ThermoFisher, USA).

2.4. In vitro drug release

Aqueous PFTV (1 mg/mL) was prepared and measured by HPLC at various time points (0, 5, 10, 20, 30 and 60 min). The vancomycin peak, suggesting release after 30 min (254 nm), was measured against a standard curve. The quantity of vancomycin released from the PFTV was calculated accordingly. Based on the amount of vancomycin released, the corresponding PFF release was calculated.

2.5. TEM test

PFTV morphology in the presence or absence of light irradiation was observed by TEM (Talos L120C, ThermoFisher, USA). Samples were deposited onto carbon-coated grids, stained with 2 % uranyl acetate for 1 min, and air-dried in a desiccator before observation.

2.6. Bacterial strains and growth conditions

Bacterial strains utilized in this study included ATCC 51299, ATCC 51559, and ATCC 51575. All strains were cultured in brain–heart infusion (BHI) broth or solid media. Bacteria were suspended from frozen storage (glycerin, −80 °C) in 10 mL BHI broth and incubated for 16–20 h. Cells were harvested by centrifugation at 3,773 g and 25 °C for 5 min.

2.7. MIC assay

A standardized broth dilution method was used to determine the bacterial MIC. Stock solutions (100 mg/mL) of the compounds and vancomycin hydrochloride were prepared in DMSO. This stock was diluted in PBS to yield the final measured concentration. Subsequently, 200 μL of this diluted stock was added to the first well of a 96-well plate and then serially diluted twofold into 100 μL PBS for a total of 10 dilutions. Overnight cultures in BHI broth were diluted to 10^6 CFU/mL and then aliquoted into the wells of a 96-well plate (100 μL/well). Each dilution series and culture treatment was performed in triplicate, with controls comprising BHI alone.

2.8. Bio-TEM experiment

To investigate bacterial changes in morphology following PFTV treatment, cells from a 5-mL overnight culture were collected by centrifugation (3,773 g, 5 min), washed three times with PBS, and resuspended in 1 mL of PBS supplemented with PFTV or PGTV. The PFTV group and PGTV group were shielded from light, whereas the PFTV + L group and PGTV + L group were exposed to NIR photoirradiation (635 nm, 500 mW/cm^2) for 10 min. A bacteria plus PBS-only control was prepared. After 4 h, the cells were collected by centrifugation, washed three times with PBS, and fixed overnight at 4 °C in 2 % paraformaldehyde/2.5 % glutaraldehyde. The fixed cells were washed three times with 0.1 M PB/cacodylate and stained with 1 % osmic acid for 1 h, followed by another round of washing. Subsequently, cells were stained with 1 % uranyl acetate for 1 h and washed three times before dehydration through an ethanol gradient. Finally, samples were embedded in resin, sectioned, stained, and observed by TEM (Talos L120C, Thermo Fisher, US).

2.9. Membrane integrity investigation

Vancomycin and PFTV (40 μM, 100 μL) were added to a suspension of VRE (10^8 CFU/mL in PBS, 100 μL). The PFTV group was kept in the dark, and the PFTV + L group was exposed to 635 nm light for 10 min. After incubation at 37 °C for 12 h, the BCA Protein Assay Kit was used to measure protein leakage as absorbance at 562 nm. After the same steps, samples were centrifuged at 3,000 g for 5 min, and the concentration of released cellular components was measured by absorbance at 260 nm.

2.10. Biofilm experiments

Overnight bacterial cultures were diluted 10^4 fold and inoculated onto 96-well plates. After 24 h, the supernatant was aspirated, and the wells were washed three times with PBS. Fresh medium was then added, and the process was repeated three times. The upper layer of the 3-day biofilm was removed and washed three times with PBS. The concentration of vancomycin, PFTV, and PGTV was 40 μM. The PFTV + L group and PGTV + L group were treated with NIR irradiation for 10 min. Following a 4-h incubation, the supernatant was discarded and replaced with 0.1 % crystal violet for 10 min of staining. After staining, the biofilms were washed three times with PBS and stained with 100 μL crystal violet dissolved in anhydrous ethanol, and absorbance was measured at 595 nm. For CLSM imaging, SYTO9 (485/498 nm) and propidium iodide (535/617 nm) fluorescent probes were used to label live and dead bacterial cells (LSM980, Zeiss).

2.11. Mouse wound excision model

Male BALB/c mice aged 6–8 weeks and weighing 22–24 g were anesthetized using a 1 % sodium pentobarbital solution. Following hair

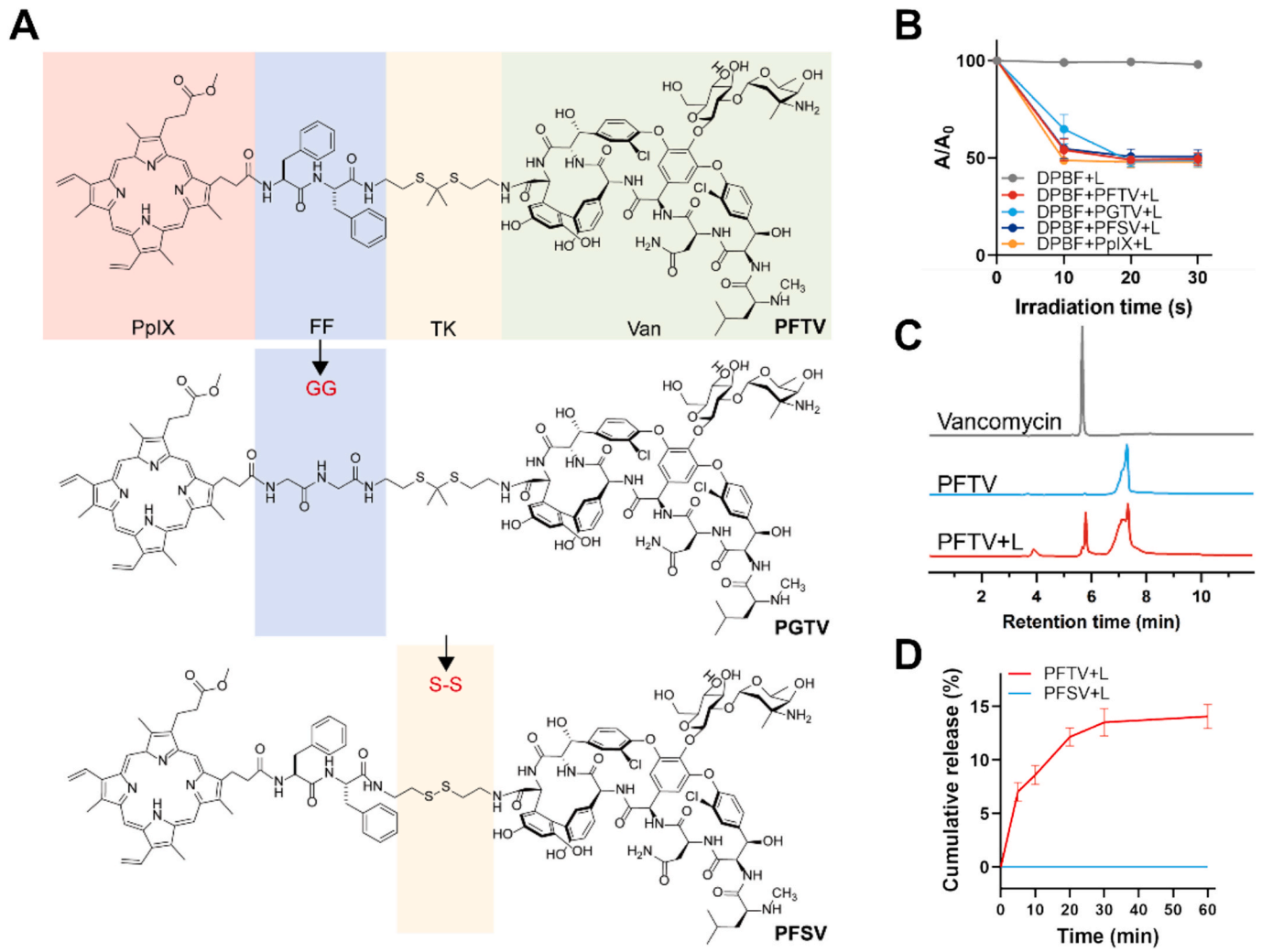

Fig. 1. NIR responsiveness and self-assembly capacity of PFTV. (A) Molecular structures of PFTV, PGTV and PFSV. (B) $^1O_2$ generation by PFTV, PGTV, PFSV, and PpIX (10 μM) using DPBF (60 μM) in PBS (635 nm, 500 mW/cm^2). (C) $^1O_2$ responsiveness of PFTV in the presence or absence of light irradiation for 10 min, detected by HPLC (635 nm, 500 mW/cm^2). (D) Cumulative PFF release from PFTV after light treatment exposure for 60 min (635 nm, 500 mW/cm^2).

removal from the back, the skin was disinfected with 70 % ethanol. Two full-thickness wounds (6 mm diameter) were created using a mouse skin punch sampler. Bacteria (1×10^8 CFU mL^{-1}) were introduced into the wound (10 μL), which was then covered using Tegaderm clear dressing (3 M). The mice were divided into four treatment groups: PBS, Van (80 μM), PFTV (80 μM), and PFTV + L (80 μM). After an infection period of 48 h, each group of mice received the designated treatment (10 μL), and the PFTV + L group underwent illumination for 10 min. The wounds were treated twice (once on day 0 and once on day 1), after which the mice were allowed to heal and observed from day 2 to day 10. Following completion of treatment, half of the mice were euthanized, and sterile PBS was used to collect a skin sample measuring approximately 1 cm × 1 cm around the wound site. The samples were homogenized and inoculated on BHI solid medium for viable bacterial counts. The remaining half of the mice continued to be monitored for wound recovery progress. All mice were euthanized after 10 days. Wound tissue and major organs (kidney, heart, spleen, lung, and liver) were examined histologically by H&E staining.

2.12. In vitro cell viability

Cytotoxicity was assessed using the MTT assay. HEK 293 T cells, L929 cells and Hacat cells were cultured in DMEM with 10 % FBS, 100 U/mL penicillin, and 100 μg/mL streptomycin at 37 °C and 5 % CO^2. Cells were seeded in 96-well plates (8×10^3 cells/well) and incubated for 24 h. The medium was replaced with 100 μL fresh medium containing varying concentrations of compounds in each well. After incubation for 24 h, the medium was replaced with 100 μL fresh medium containing MTT (5 mg/mL) and incubated for 4 h. Subsequently, 100 μL SDS-HCl (10 % SDS + 0.01 M HCl) was added to each well, followed by overnight incubation at 37 °C to halt the reaction and dissolve the formazan. Absorbance was measured at 595 nm using a microplate reader (Varioskan Lux, ThermoFisher). Experiments were performed in triplicate, and results were reported as means and standard deviation (SD).

2.13. In vitro Hemolysis assay

Fresh rabbit blood was centrifuged at 2,000 g for 5 min to separate the red blood cells (RBCs), which were then washed three times with PBS and suspended in PBS (8%). The test compounds in PBS were mixed in a 1:1 ratio with the RBCs. TritonX-100 plus RBCs served as the positive control, whereas PBS plus RBCs served as the negative control. All samples were incubated at 37 °C for 3 h and then centrifuged at 2,000 g for 5 min. The supernatant (100 μL) was carefully removed, and absorbance was measured at 570 nm.

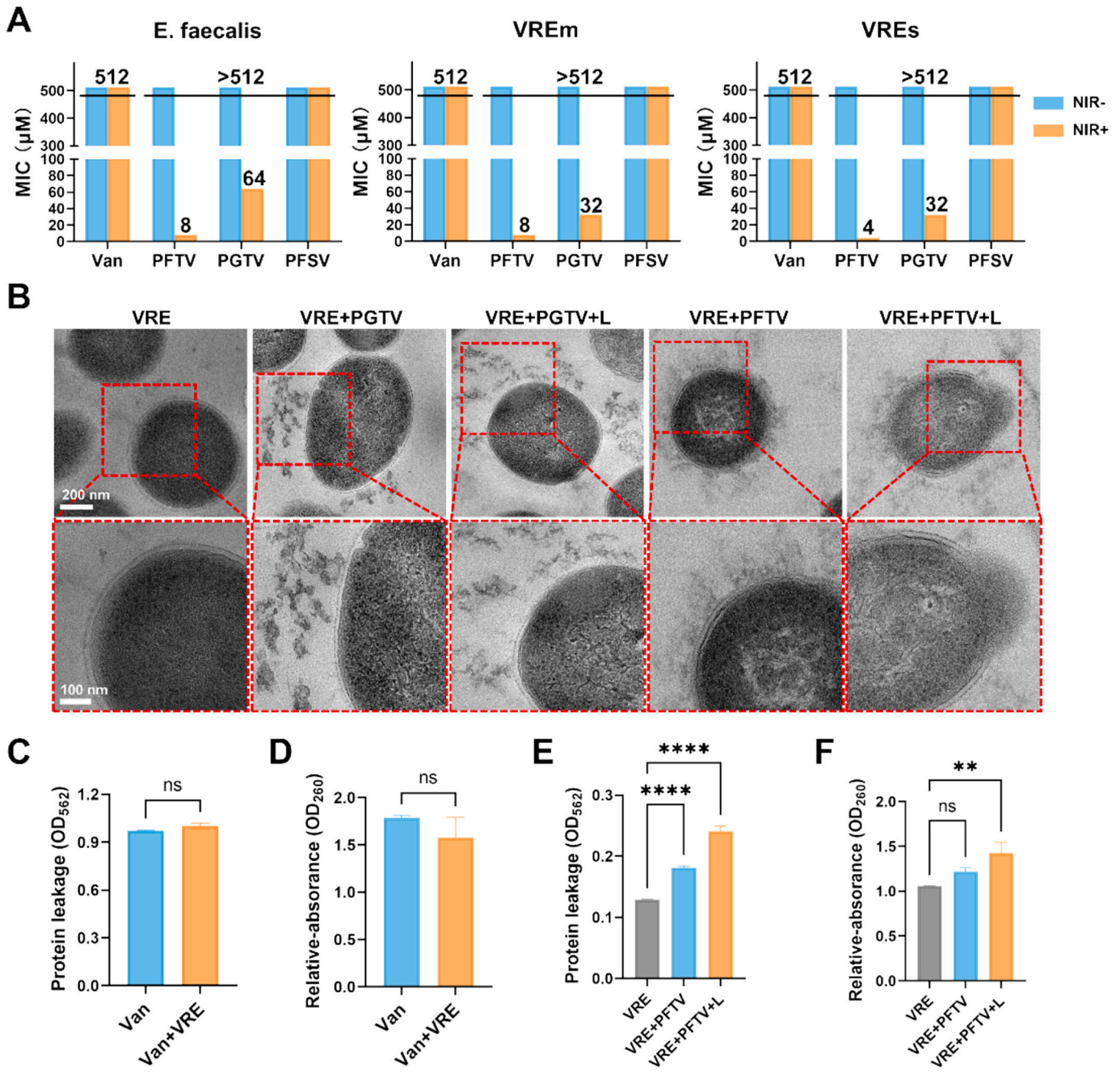

Fig. 2. NIR-driven antibacterial efficacy of PFTV against VREs. (A) MICs of vancomycin, PFTV, PGTV, and PFSV against VREs in the presence or absence of NIR (635 nm, 500 mW/cm^2) for 10 min. (B) Bio-TEM images of untreated and treated VRE. NIR (635 nm, 500mW/cm^2) for 10 min. (C) Protein and (D) DNA leakage from Van-treated VRE (n = 3/group) (*t*-test; *p < 0.05, **p < 0.01, ***p < 0.001). (E) Protein and (F) DNA leakage from PFTV-treated VRE with or without NIR irradiation (n = 3/group) (one-way ANOVA; *p < 0.05, **p < 0.01, ***p < 0.001, ****p < 0.0001). NIR (635 nm, 500 mW/cm^2) for 10 min.

2.14. Statistical analysis

All data are expressed as the mean ± SD of triplicate experiments. Statistical significance ($p < 0.05$) was assessed by *t*-test or one-way ANOVA. In all tests, statistical significance was set at *p < 0.05, **p < 0.01, ***p < 0.001, and ****p < 0.0001. A p value < 0.05 was defined as statistically significant.

3. Results and discussion

3.1. Synthesis and characterization of peptide-vancomycin conjugates

The synthetic route for PFTV involved three key steps (Fig. S1). First, the short peptide conjugates of PFF were synthesized using solid-phase peptide synthesis. In the subsequent step, vancomycin reacted with TK to form an amide bond, yielding Van-TK-NH_2. The final step involved linking the carboxyl group of PFF to the amino group of Van-TK-NH_2, resulting in the formation of PFTV. Control compounds PpIX-GG-TK-Van (PGTV), which exhibits significantly weaker self-assembly properties post-TK cleavage, and PpIX-FF-SS-Van (PFSV), which does not undergo light-induced structural transformation, were synthesized using the same methodology. The chemical structures of all compounds are illustrated in Fig. 1A. All compounds were purified by high-performance liquid chromatography (HPLC) and characterized by liquid chromatography–mass spectrometry (Figs. S2 and S3).

Compounds were assessed for their $^1O_2$ production capacity using

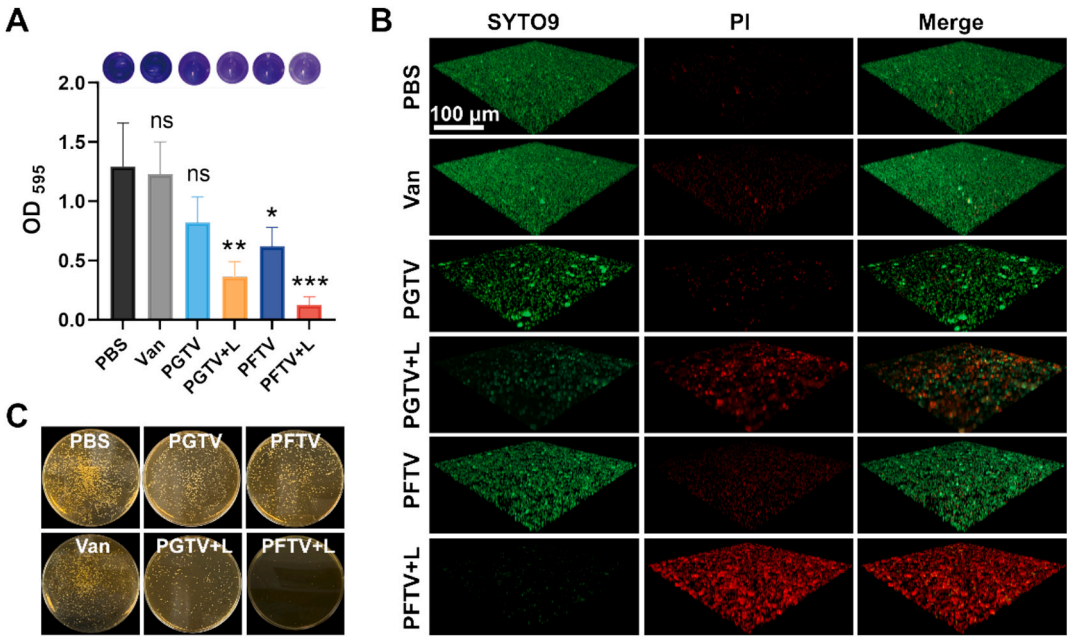

Fig. 3. Evaluation of PFTV to remove VRE biofilms. NIR (635 nm, 500 mW/cm^2) for 10 min. (A) Crystal violet staining of VRE biofilms treated with PBS, vancomycin, PGTV, and PFTV in the presence and absence of NIR irradiation (n = 3/group) (one-way ANOVA; *p < 0.05, **p < 0.01, ***p < 0.001). (B) Representative CLSM images of biofilms labeled with SYTO9/PI for live (green) and dead (red) cells. (C) Colony growth of VRE after various treatments. (For interpretation of the references to colour in this figure legend, the reader is referred to the web version of this article.)

the 1,3-diphenylisobenzofuran (DPBF) probe under light irradiation (635 nm) [48]. As shown in Fig. 1B, absorbance decreased with increasing illumination time for all compounds except DPBF, suggesting that the $^1O_2$-generating capacity of PpIX was unaffected by the peptide modification and the presence of vancomycin. HPLC was used to monitor PFF release from PFTV under light irradiation. As shown in Fig. 1C, a single peak corresponding to PFTV was observed in the absence of light. However, under light irradiation, $^1O_2$ generated by photoexcited PpIX triggered cleavage of the TK linker, resulting in the appearance of another peak with a retention time consistent with vancomycin. In contrast, the compound PFSV, which substitutes the TK bond with a disulfide bond, exhibited no changes in its HPLC spectrum before and after light irradiation (Fig. S4). Quantitative results demonstrated that the release of PFF increased with the duration of irradiation (Fig. 1D). After 60 min of light exposure, PFTV released 14 % of the PFF. Additionally, the structural response to NIR irradiation was examined by investigating the ultramicro-morphologies formed by various compounds before and after light exposure. Transmission electron microscopy (TEM) images revealed that PFTV formed dispersed circular aggregates before light irradiation, then transformed into regular fibrous structures upon exposure (Fig. S5). In contrast, PGTV and PFSV showed no significant formation of nanostructures or changes in morphology before and after light irradiation, which can be attributed to their respective chemical structures.

3.2. Antibacterial activity and mechanism investigation

Minimum inhibitory concentrations (MICs) were determined using the broth microdilution method. Results indicated that vancomycin possessed an extremely high MIC of 512 μM against three VRE bacterial isolates (Table S1, Fig. 2A). All the compounds themselves exhibited little to no antibacterial activity against VRE in the absence of NIR irradiation. In contrast, PFTV and PGTV exhibited significant anti-VRE activity upon NIR light exposure. The growth inhibition property against VRE of PFTV could maximumly improve by more than 100-folds, exhibited as its MIC value was reduced to as low as 4–8 μM. This level of improvement suggests that our approach could potentially overcome the high resistance threshold of VRE, making it possible to achieve therapeutic efficacy at much lower drug concentrations. Such a reduction is particularly relevant in clinical settings where high antibiotic doses are often associated with toxicity and side effects [49]. In contrast, the MIC value of PGTV was only reduced to 32–64 μM, which may attributed to its considerably weaker self-assembly capacity on VRE membrane after NIR treatment. In addition, PFSV exhibited virtually no antibacterial activity against VREs even at 512 μM with NIR irradiation, demonstrating that the produced $^1O_2$ in extracellular had a negligible antibacterial effect.

To investigate the potential antibacterial mechanism of peptide-vancomycin conjugates on VRE, Bio-TEM was used to observe the morphology of VRE under various treatment conditions. As shown in Fig. 2B, the untreated VRE exhibited smooth, intact membrane structures. Although treatment with PGTV triggered low-level aggregate formation on the cell surface, the cell membrane remained largely intact before and after NIR light irradiation, suggesting weak target binding and in situ assembly properties. In contrast, after treating with PFTV, a large amount of aggregates accumulated on the bacterial surface. Upon NIR light irradiation, the local accumulation of aggregates on bacterial surface was further enhanced causing destructed cell membrane, which could be attributed to the released PFF and the residual PFTV simultaneously in situ co-assembly on VRE. Moreover, the leakage of proteins and nucleic acids from bacteria was detected. The results in Fig. 2C and D indicated that no protein and DNA leakage was detected in VRE treated with free vancomycin. In contrast, PFTV with NIR promoted more protein and DNA leakage compared to PFTV alone and vancomycin itself (Fig. 2E and F), ultimately leading to bacterial death. These findings suggest that PFTV retained its membrane-targeting ability and self-assembled in situ into nanoantibacterial agents upon NIR excitation, which could induce cell death by disrupting the bacterial cell membrane and causing loss of intracellular content.

3.3. VRE biofilm eradication evaluation in vitro

Biofilms formed by pathogenic bacteria have long been recognized as significant contributors to the resistance observed against antimicrobial

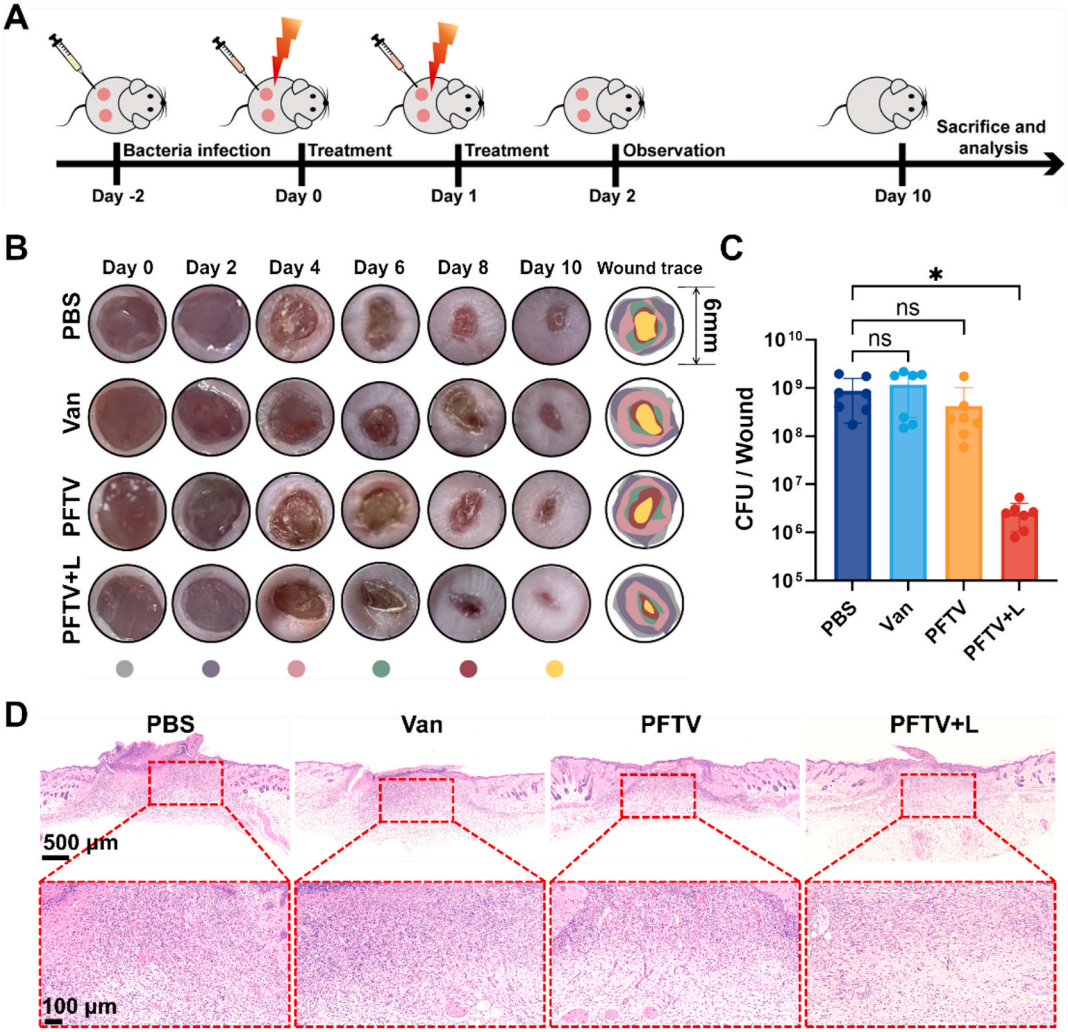

Fig. 4. PFTV activity in a murine wound model of VRE infection. NIR (635 nm, 500 mW/cm^2) for 10 min. (A) Schematic diagram of the model. (B) Photographs and schematic diagram of wound closure on days 0, 2, 4, 6, 8, and 10. (C) VRE counts (CFU/wound) in the wounds on day 2 (n = 7) (one-way ANOVA; *p < 0.05, **p < 0.01, ***p < 0.001). (D) H&E staining of wound tissues after different treatments on day 10.

agents [50–52]. The antibacterial effectiveness of PFTVs against VRE biofilms was assessed. As shown in Fig. 3A, free vancomycin and PGTV alone exhibited negligible biofilm eradication capabilities, as evidenced by the quantitative analysis of crystal violet staining, showing no significant difference compared to the control. However, following NIR light irradiation, the PGTV treatment demonstrated some biofilm removal, which was consistent with its in vitro antibacterial results. Notably, only the PFTV treatment successfully eliminated more than 50 % of the biofilm, achieving an impressive eradication rate of approximately 90 % when combined with NIR irradiation.

To further elucidate the efficacy of various treatments in eradicating VRE biofilms, SYTO9/PI labeling was employed to distinguish viable from dead bacteria. Confocal laser scanning microscopy (CLSM) images (Fig. 3B) revealed strong green fluorescence in the free vancomycin and PBS-treated groups, suggesting that free vancomycin exhibited minimal efficacy in biofilm removal. In contrast, the PGTV and PFTV treatment groups showed some dead bacteria within the biofilms, with the number of dead bacteria increasing upon exposure to NIR light, evidenced by a reduction in green fluorescence and a corresponding enhancement in red fluorescence. Notably, the established biofilm was approximately 100 % cleared following treatment with PFTV in conjunction with NIR light. Additionally, colony-forming units (CFUs) were analyzed and quantified following various treatments. PFTV combined with NIR irradiation produced a robust antibacterial effect (Figs. 3C and S6). Compared to the control group, the PFTV plus NIR group demonstrated a reduction of viable bacteria by more than 2 log-fold, achieving a killing rate exceeding 99 %. These findings further underscore that the NIR-triggered PFTV in situ self-assembly significantly enhances antibacterial efficacy and facilitates effective biofilm removal.

3.4. Wound repair in a VRE skin infection model

Given the observed antibacterial activity of PFTV in vitro, a VRE skin infection model was established using BALB/c mice to evaluate its potential efficacy in treating traumatic infections. The treatment process is illustrated in Fig. 4A. The wound recovery photos shown in Fig. 4B indicated that, over time, free vancomycin and PFTV treatments had minimal effect on promoting wound healing when compared to the PBS group. On day 2, wounds in the PBS, Van, and PFTV groups still exhibited exudate, which can lead to maceration of the surrounding skin. In contrast, the PFTV + L group showed almost no wound exudate, demonstrating better wound recovery following treatment. The wounds treated with PFTV combined with NIR light exhibited visible scabbing by the sixth day, achieving an average healing rate of approximately 95 % on day 10, whereas the control groups (PBS, vancomycin, and PFTV) achieved only ≈ 77–81 % closure (Fig. S7). Additionally, a quantitative analysis of CFU after different treatments was performed. As depicted in Fig. 4C, the CFU of the vancomycin treated group had escalated to nearly

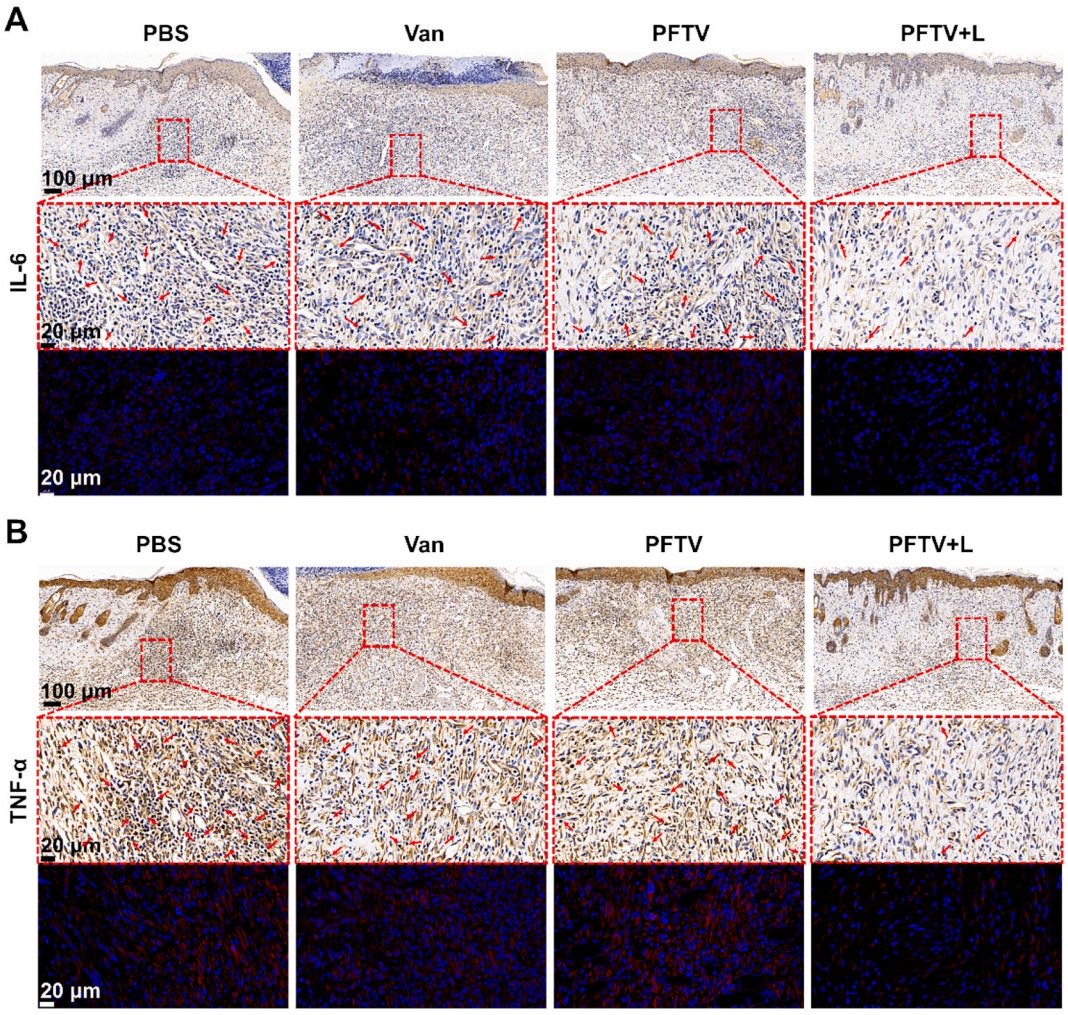

Fig. 5. Immunohistochemical staining (brown) and immunofluorescent staining (red) of (A) IL-6 and (B) TNF-α in the subcutaneous tissue of wounds after different treatments on day 10. Red arrows indicate IL-6 positive cells and TNF-α positive cells. (For interpretation of the references to colour in this figure legend, the reader is referred to the web version of this article.)

10^9, similar to that of PBS treated group, suggesting that free vancomycin did not manifest any in vivo antibacterial efficacy against VRE. Conversely, the CFU count in the PFTV-treated group under NIR light irradiation was only 10^6, suggesting that over two orders of magnitude of bacteria on the wound were effectively eradicated.

An exaggerated inflammatory response often accompanies wound infections and has been considered a key contributor to delayed wound healing [53,54]. Histological examination was conducted to evaluate the progression of wound healing following different treatments. The results of hematoxylin and eosin (H&E) staining revealed pronounced infiltration of macrophages and lymphocytes within the dermal layer of the skin in the PBS, vancomycin, and PFTV without NIR-treated groups, suggesting serious inflammatory responses in the established wound model (Fig. 4D). In contrast, the PFTV plus NIR-treated group exhibited a lack of significant inflammatory infiltration. The expression of proinflammatory cytokines, such as interleukin 6 (IL-6) and tumor necrosis factor α (TNF-α), was further assessed by immunohistochemical staining. Dysregulation of these inflammatory mediators can adversely impact fibroblast functions, including proliferation and migration, thereby affecting wound healing [55]. High secretion of IL-6 and TNF-α was observed in skin treated with PBS, vancomycin, and PFTV, suggesting an excessive presence of inflammatory cells. Conversely, significantly lower levels of IL-6 and TNF-α were observed in the PFTV plus NIR group, suggesting an effective reduction in the inflammatory response at the wound site (Fig. 5). Specifically, compared to the PBS group, the positive areas of IL-6 and TNF-α in the PFTV + L group were reduced by 50 % and 70 %, respectively (Fig. S8), which is critical for preventing chronic inflammation and promoting healing [56,57].

Collagen formation is a crucial step in the wound healing process [58,59]. Masson staining was performed to evaluate collagen remodeling and maturation in the skin infection model. Unlike free vancomycin and PFTV alone, the combination of PFTV and NIR therapy led to a more extensive and orderly arrangement of collagen fibers, suggesting its superior efficacy in promoting tissue recovery (Fig. 6A). Specifically, the collagen area in the PBS group was approximately 25 %, while in the PFTV + L group, it increased to approximately 40 %. (Fig. S9) In addition, angiogenesis, refering to neovascularization originate from the preexisting vascular system, also represents a prominent hallmark of wound healing and proliferation [60]. Skin specimens were collected on day 10, and neovascularization was assessed using CD31 and α-smooth muscle actin (α-SMA) immunostaining. As shown in Fig. 6B, neither PBS nor PFTV alone yielded observable signs of neovascularization. However, the PFTV plus NIR model displayed noticeable indications of new blood vessel generation, which was in accordance with their ability in promoting wound healing, as these newly formed vessels could facilitate oxygen and nutrient supply. Collectively, these results indicate that the PFTV plus NIR treatment effectively accelerates wound healing by inhibiting bacterial growth, reducing inflammatory responses, and promoting neovascularization.

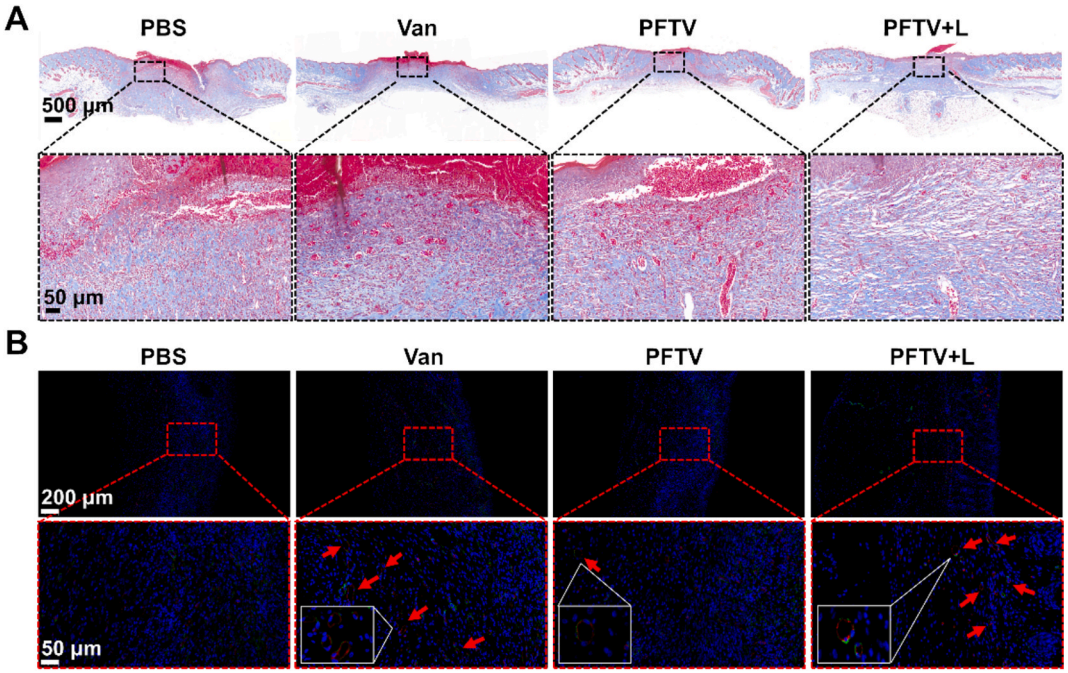

Fig. 6. (A) Masson staining of the infected skins harvested from different groups on day 10. (B) Immunofluorescence images showing CD31 (red) and α-SMA (green) in the infected wounds on day 10 after different treatments. Red arrows indicate neovascularization. (For interpretation of the references to colour in this figure legend, the reader is referred to the web version of this article.)

3.5. Biocompatibility evaluation

To establish the biocompatibility of PFTV with healthy cells, cytotoxicity was assessed by MTT assay in human embryonic kidney cells (HEK 293 T). As shown in Fig. S10, free vancomycin significantly decreased cell viability of HEK 293 T at half-MIC, which was consistent with previous studies on the nephrotoxicity of vancomycin [44,61]. In contrast, PFTV showed almost no cytotoxicity against the normal cells. Additionally, we evaluated the cytotoxicity of PFTV on skin cells, including fibroblasts and keratinocytes (Fig. S11). The results demonstrated that PFTV exhibited no toxicity to either cell type at the tested concentrations. Hemolysis assays were performed to characterize the potential for PFTV-induced side effects, and results revealed no hemolytic activity, even at 512 μM (Fig. S12). Additionally, histological analysis of the major organs (heart, liver, spleen, lung, and kidney) was performed in wound-infected mice after 10 days of treatment. H&E staining revealed typical morphological characteristics in the organs of PFTV-treated mice (Fig. S13), suggesting the absence of histological toxicity associated with PFTV treatment. Therefore, PFTV demonstrated a favorable biocompatibility profile, making it suitable for anti-bacterial infection applications in vivo.

4. Conclusions

In summary, we have developed a NIR light–responsive system of peptide-vancomycin conjugate to address antibiotic-resistant bacterial infections. As an amphiphilic precursor molecule, the conjugate underwent hydrophobic–hydrophilic phase transformation upon NIR light irradiation, resulting in the in situ self-assembly and formation of a multivalent nanoantibacterial agent on the VRE cell surface. Compared to free vancomycin, the PFTV combined with NIR light demonstrated over a 60-fold reduction in MIC against VRE and achieved an impressive 99 % clearance rate of VRE biofilm through the in situ generation of a peptide-based nanoagent. Furthermore, this conjugate, along with NIR light, exhibited significant wound healing properties and favorable biocompatibility, showing no toxicity or damage to skin tissue. In future, we plan to further optimize the material for broader-spectrum activity, including Gram-negative bacteria, and evaluate its efficacy in more complex infection models. While our results are promising, we acknowledge that challenges remain in scaling up production and achieving consistent performance in clinical settings. The potential impact of host immune responses and the need for precise control of NIR irradiation parameters are also critical considerations for clinical translation. Nevertheless, we have demonstrated the efficacy of a novel NIR-activated in situ self-assembly strategy to treat VRE infection, which could provide new paradigms and inspirations for the development of nanoantibiotics and therapies for MDR bacterial infections.

CRediT authorship contribution statement

Yu Zhang: Writing – review & editing, Resources, Funding acquisition, Conceptualization. **Chunhua Ren:** Writing – review & editing, Methodology, Funding acquisition, Conceptualization. **Huayang Liu:** Software, Investigation. **Jingyi Duan:** Software, Methodology. **Mengyao Wang:** Investigation. **Ziao Zhou:** Software, Methodology. **Jinyou Duan:** Writing – review & editing, Resources, Methodology. **Huaimin Wang:** Writing – review & editing, Supervision, Funding acquisition. **Xiaoli Zhang:** Writing – review & editing, Resources, Funding acquisition, Conceptualization.

Declaration of competing interest

The authors declare that they have no known competing financial interests or personal relationships that could have appeared to influence the work reported in this paper.

Acknowledgments

This project was supported by the National Natural Science Foundation of China (51703181, 82272145), and Foundation of Westlake University and Tencent Foundation. We thank the Instrumentation and Service Center for Molecular Sciences, Instrumentation and Service Center for Physical Sciences, General Equipment Core Facility, Biomedical Research Core Facilities, and Laboratory Animal Resource

Center at Westlake University for the assistance with measurements. Mice were handled in accordance with institutional guidelines, and all animal studies were approved by the Institutional Animal Care and Use Committee (IACUC) of Westlake University (IACUC Protocol # AP#24-004-WHM).

Appendix A. Supplementary data

Supplementary data to this article can be found online at https://doi.org/10.1016/j.cej.2025.161303.

Data availability

Data will be made available on request.

References

[1] Z. Ling, X. Liu, S. Cheng, C. Jiang, W. Zhao, C. Zhao, Rational design of hemocompatible hydrogel microspheres towards pathogen-associated molecular patterns removal for gram-positive bacteria-induced sepsis, Chem. Eng. J. 489 (2024) 151461, https://doi.org/10.1016/j.cej.2024.151461.
[2] S. Panthong, K. Takkavatakarn, P. Sitticharoenchai, Clinical risk factors and prediction model for infective endocarditis in patients with gram-positive bacteremia, Eur. Heart J. 44(Supplement_2) (2023) ehad655. 1774. https://doi.org/10.1093/eurheartj/ehad655.1774.
[3] A.G. Myers, R.B. Clark, Discovery of macrolide antibiotics effective against multi-drug resistant gram-negative pathogens, Acc. Chem. Res. 54 (7) (2021) 1635–1645, https://doi.org/10.1021/acs.accounts.1c00020.
[4] J.J. Seo, N. Mandakhbayar, M.S. Kang, J.-Y. Yoon, N.-H. Lee, J. Ahn, H.-H. Lee, J.-H. Lee, H.-W. Kim, Antibacterial, proangiogenic, and osteopromotive nanoglass paste coordinates regenerative process following bacterial infection in hard tissue, Biomaterials 268 (2021) 120593, https://doi.org/10.1016/j.biomaterials.2020.120593.
[5] J. Grapsa, C. Blauth, Y. Chandrashekhar, B. Prendergast, B. Erb Jr, M. Mack, V. Fuster, Staphylococcus aureus infective endocarditis: Jacc patient pathways, J. Am. Coll. Cardiol. 79 (1) (2022) 88–99, https://doi.org/10.1016/j.jacc.2021.10.015.
[6] R. Gaynes, The discovery of penicillin—new insights after more than 75 years of clinical use, Emerg. Infect. Dis. 23 (5) (2017) 849, https://doi.org/10.3201/eid2305.161556.
[7] M.A. Cook, G.D. Wright, The past, present, and future of antibiotics, Sci. Transl. Med. 14 (657) (2022) eabo7793, https://doi.org/10.1126/scitranslmed.abo7793.
[8] S. Li, M. Lu, C. Dai, B. Xu, N. Wu, L. Wang, C. Liu, F. Chen, H. Yang, Z. Huang, Advanced palladium nanosheet-enhanced phototherapy for treating wound infection caused by multidrug-resistant bacteria, Small (2024) 2407180, https://doi.org/10.1002/smll.202407180.
[9] S.P. Hameed, H. Kotakonda, S. Sharma, R. Nandishaiah, N. Katagihallimath, R. Rao, C. Sadler, I. Slater, M. Morton, A. Chandrasekaran, Bwc0977, a broad-spectrum antibacterial clinical candidate to treat multidrug resistant infections, Nat. Commun. 15 (1) (2024) 8202, https://doi.org/10.1038/s41467-024-52557-2.
[10] C.R. MacNair, S.T. Rutherford, M.-W. Tan, Alternative therapeutic strategies to treat antibiotic-resistant pathogens, Nat. Rev. Microbiol. 22 (5) (2024) 262–275, https://doi.org/10.1038/s41579-023-00993-0.
[11] S. Walesch, J. Birkelbach, G. Jézéquel, F.J. Haeckl, J.D. Hegemann, T. Hesterkamp, A.K. Hirsch, P. Hammann, R. Müller, Fighting antibiotic resistance—strategies and (pre) clinical developments to find new antibacterials, EMBO Rep. 24 (1) (2023) e56033, https://doi.org/10.15252/embr.202256033.
[12] M. Lakemeyer, W. Zhao, F.A. Mandl, P. Hammann, S.A. Sieber, Thinking outside the box—novel antibacterials to tackle the resistance crisis, Angew. Chem. Int. Ed. 57 (44) (2018) 14440–14475, https://doi.org/10.1002/anie.201804971.
[13] C.-H. Wang, Y.-H. Hsieh, Z.M. Powers, C.-Y. Kao, Defeating antibiotic-resistant bacteria: Exploring alternative therapies for a post-antibiotic era, Int. J. Mol. Sci. 21 (3) (2020) 1061, https://doi.org/10.3390/ijms21031061.
[14] X. Wan, J. Xiao, M. Yin, Y. Yao, J. Luo, Counterion-induced antibiotic-based small-molecular micelles for methicillin-resistant staphylococcus aureus infections, Acta Biomater. 166 (2023) 627–639, https://doi.org/10.1016/j.actbio.2023.05.029.
[15] J. Ding, J. Zhang, J. Li, D. Li, C. Xiao, H. Xiao, H. Yang, X. Zhuang, X. Chen, Electrospun polymer biomaterials, Prog. Polym. Sci. 90 (2019) 1–34, https://doi.org/10.1016/j.progpolymsci.2019.01.002.
[16] X.L. Hu, L. Chu, X. Dong, G.R. Chen, T. Tang, D. Chen, X.P. He, H. Tian, Multivalent glycosheets for double light–driven therapy of multidrug-resistant bacteria on wounds, Adv. Funct. Mater. 29 (14) (2019) 1806986, https://doi.org/10.1002/adfm.201806986.
[17] F.R. Xu, G.L. Zhang, K. Zhang, P. Chen, Q. Wang, Y. Pan, B.Z. Tang, H.T. Feng, Wide-spectrum nano-antibiotics based on tpa-py@ auncs⊂ bsa for multimodal synergistic therapy of drug-resistant bacteria and wound infections, Aggregate (2024) e699, https://doi.org/10.1002/agt2.699.
[18] M. Xie, M. Gao, Y. Yun, M. Malmsten, V.M. Rotello, R. Zboril, O. Akhavan, A. Kraskouski, J. Amalraj, X. Cai, Antibacterial nanomaterials: Mechanisms, impacts on antimicrobial resistance and design principles, Angew. Chem. Int. Ed. 62 (17) (2023) e202217345, https://doi.org/10.1002/anie.202217345.
[19] Y. Wang, Y. Yang, Y. Shi, H. Song, C. Yu, Antibiotic-free antibacterial strategies enabled by nanomaterials: Progress and perspectives, Adv. Mater. 32 (18) (2020) 1904106, https://doi.org/10.1002/adma.202070138.
[20] J.M.V. Makabenta, A. Nabawy, C.-H. Li, S. Schmidt-Malan, R. Patel, V.M. Rotello, Nanomaterial-based therapeutics for antibiotic-resistant bacterial infections, Nat. Rev. Microbiol. 19 (1) (2021) 23–36, https://doi.org/10.1038/s41579-020-0420-1.
[21] Z. Geng, Z. Cao, J. Liu, Recent advances in targeted antibacterial therapy basing on nanomaterials, Exploration 3 (1) (2023) 20210117, https://doi.org/10.1002/exp.20210117.
[22] C. He, P. Feng, M. Hao, Y. Tang, X. Wu, W. Cui, J. Ma, C. Ke, Nanomaterials in antibacterial photodynamic therapy and antibacterial sonodynamic therapy, Adv. Funct. Mater. (2024) 2402588, https://doi.org/10.1002/adfm.202402588.
[23] R. Kang, Y. Zhuang, M. Liu, Application of alginate in inflammatory bowel disease, Biomed. Eng. Commun. 3 (2) (2024) 9, https://doi.org/10.53388/BMEC2024009.
[24] Q. Yu, C. Wang, X. Zhang, H. Chen, M.X. Wu, M. Lu, Photochemical strategies toward precision targeting against multidrug-resistant bacterial infections, ACS Nano (2024), https://doi.org/10.1021/acsnano.3c12714.
[25] C.K. Dzuvor, Toward clinical applications: Transforming nonantibiotic antibacterials into effective next-generation supramolecular therapeutics, ACS Nano 18 (4) (2024) 2564–2577, https://doi.org/10.1021/acsnano.3c11045.
[26] J. Xiao, M. Yin, M. Yang, J. Ren, C. Liu, J. Lian, X. Lu, Y. Jiang, Y. Yao, J. Luo, Lipase and ph-responsive diblock copolymers featuring fluorocarbon and carboxyl betaine for methicillin-resistant staphylococcus aureus infections, J. Control. Release 369 (2024) 39–52, https://doi.org/10.1016/j.jconrel.2024.03.021.
[27] S.-Y. Qin, J.-Q. Feng, Y.-J. Cheng, W.-L. Liu, A.-Q. Zhang, L. Wang, H. Wang, X.-Z. Zhang, A comprehensive review on peptide-bearing biomaterials: From ex situ to in situ self-assembly, Coord. Chem. Rev. 502 (2024) 215600.
[28] L.L. Li, H.L. Ma, G.B. Qi, D. Zhang, F. Yu, Z. Hu, H. Wang, Pathological-condition-driven construction of supramolecular nanoassemblies for bacterial infection detection, Adv. Mater. 28 (2) (2016) 254–262, https://doi.org/10.1002/adma.201503437.
[29] Z. Wang, Q. Wang, H. Cao, Z. Wang, D. Wang, J. Liu, T. Gao, C. Ren, J. Liu, Mitochondrial localized in situ self-assembly reprogramming tumor immune and metabolic microenvironment for enhanced cancer therapy, Adv. Mater. 36 (15) (2024) 2311043, https://doi.org/10.1002/adma.202311043.
[30] H.W. An, M. Mamuti, X. Wang, H. Yao, M.D. Wang, L. Zhao, L.L. Li, Rationally designed modular drug delivery platform based on intracellular peptide self-assembly, Exploration 1 (2) (2021) 20210153, https://doi.org/10.1002/exp.20210153.
[31] J. Kim, S. Lee, Y. Kim, M. Choi, I. Lee, E. Kim, C.G. Yoon, K. Pu, H. Kang, J.S. Kim, In situ self-assembly for cancer therapy and imaging, Nat. Rev. Mater. 8 (11) (2023) 710–725, https://doi.org/10.1038/s41578-023-00589-3.
[32] H. Huang, Y. Zheng, M. Chang, J. Song, L. Xia, C. Wu, W. Jia, H. Ren, W. Feng, Y. Chen, Ultrasound-based micro-/nanosystems for biomedical applications, Chem. Rev. 124 (13) (2024) 8307–8472, https://doi.org/10.1021/acs.chemrev.4c00009.
[33] Q. Han, J.W. Lau, T.C. Do, Z. Zhang, B. Xing, Near-infrared light brightens bacterial disinfection: Recent progress and perspectives, ACS Appl. Bio Mater. 4 (5) (2021) 3937–3961, https://doi.org/10.1021/acsabm.0c01341.
[34] H. Gao, X. Qi, J. Zhang, N. Wang, J. Xin, D. Jiao, K. Liu, J. Qi, Y. Guan, D. Ding, Smart one-for-all agent with adaptive functions for improving photoacoustic /fluorescence imaging-guided photodynamic immunotherapy, Small Methods 7 (5) (2023) e2201582, https://doi.org/10.1002/smtd.202201582.
[35] F.M. Yavitt, B.E. Kirkpatrick, M.R. Blatchley, K.F. Speckl, E. Mohagheghian, R. Moldovan, N. Wang, P.J. Dempsey, K.S. Anseth, In situ modulation of intestinal organoid epithelial curvature through photoinduced viscoelasticity directs crypt morphogenesis, Sci. Adv. 9 (3) (2023) eadd5668, https://doi.org/10.1126/sciadv.add5668.
[36] Y. Chen, S. Wang, F. Zhang, Near-infrared luminescence high-contrast in vivo biomedical imaging, Nat. Rev. Bioeng. 1 (1) (2023) 60–78.
[37] R. Ma, N. Alifu, Z. Du, S. Chen, Y. Heng, J. Wang, L. Zhu, C. Ma, X. Zhang, Indocyanine green-based theranostic nanoplatform for nir fluorescence image-guided chemo/photothermal therapy of cervical cancer, Int. J. Nanomed. 16 (null) (2021) 4847–4861, https://doi.org/10.2147/IJN.S318678.
[38] B.J. Kim, B. Xu, Enzyme-instructed self-assembly for cancer therapy and imaging, Bioconjug. Chem. 31 (3) (2020) 492–500, https://doi.org/10.1021/acs.bioconjchem.0c00025.
[39] X. Wei, J. Huang, C. Zhang, C. Xu, K. Pu, Y. Zhang, Highly bright near-infrared chemiluminescent probes for cancer imaging and laparotomy, Angew. Chem., Int. Ed. 62 (8) (2023) e202213791.
[40] J. Huang, K. Pu, Activatable molecular probes for second near-infrared fluorescence, chemiluminescence, and photoacoustic imaging, Angew. Chem. Int. Ed. 59 (29) (2020) 11717–11731, https://doi.org/10.1002/ange.202001783.
[41] Y. Wang, Y. Feng, H. Tu, H. Zheng, Y. Xiang, T. Zhang, X. Huang, F. Lu, K. Yu, E. Hu, Photothermal-manipulatable shape memory polyacrylamide/gelatin janus hydrogel with drug carrier array for invasive wound closure and responsive drug release, Int. J. Biol. Macromol. 293 (2025) 139255.
[42] C. Yang, C. Ren, J. Zhou, J. Liu, Y. Zhang, F. Huang, D. Ding, B. Xu, J. Liu, Dual fluorescent- and isotopic-labelled self-assembling vancomycin for in vivo imaging of bacterial infections, Angew. Chem. Int. Ed. Engl. 56 (9) (2017) 2356–2360, https://doi.org/10.1002/anie.201610926.
[43] X. Ning, S. Lee, Z. Wang, D. Kim, B. Stubblefield, E. Gilbert, N. Murthy, Maltodextrin-based imaging probes detect bacteria in vivo with high sensitivity and specificity, Nat. Mater. 10 (8) (2011) 602–607, https://doi.org/10.1038/nmat3074.

[44] A. Ottonello, J.A. Wyllie, O. Yahiaoui, S. Sun, R.A. Koelln, J.A. Homer, R. M. Johnson, E. Murray, P. Williams, J.R. Bolla, C.V. Robinson, T. Fallon, T. P. Soares da Costa, J.E. Moses, Shapeshifting bullvalene-linked vancomycin dimers as effective antibiotics against multidrug-resistant gram-positive bacteria, Proc. Natl. Acad. Sci. U.S.A. 120 (15) (2023) e2208737120, https://doi.org/10.1073/pnas.2208737120.

[45] X. Yan, P. Zhu, J. Li, Self-assembly and application of diphenylalanine-based nanostructures, Chem. Soc. Rev. 39 (6) (2010) 1877–1890, https://doi.org/10.1039/b915765b.

[46] W. Ji, Y. Tang, P. Makam, Y. Yao, R. Jiao, K. Cai, G. Wei, E. Gazit, Expanding the structural diversity and functional scope of diphenylalanine-based peptide architectures by hierarchical coassembly, J. Am. Chem. Soc. 143 (42) (2021) 17633–17645, https://doi.org/10.1021/jacs.1c07915.

[47] H. He, L. Du, H. Xue, J. Wu, X. Shuai, Programmable therapeutic nanoscale covalent organic framework for photodynamic therapy and hypoxia-activated cascade chemotherapy, Acta Biomater. 149 (2022) 297–306, https://doi.org/10.1016/j.actbio.2022.07.003.

[48] W. Feng, Y. Lv, Z. Chen, F. Wang, Y. Wang, Y. Pei, W. Jin, C. Shi, Y. Wang, Y. Qu, W. Ji, L. Pu, X.-W. Liu, Z. Pei, A carrier-free multifunctional nano photosensitizer based on self-assembly of lactose-conjugated bodipy for enhanced anti-tumor efficacy of dual phototherapy, Chem. Eng. J. 417 (2021), https://doi.org/10.1016/j.cej.2021.129178.

[49] S. Van Hal, T.P. Lodise, D. Paterson, The clinical significance of vancomycin minimum inhibitory concentration in staphylococcus aureus infections: A systematic review and meta-analysis, Clin. Infect. Dis. 54 (6) (2012) 755–771.

[50] S. Liu, H. Lu, S. Zhang, Y. Shi, Q. Chen, Phages against pathogenic bacterial biofilms and biofilm-based infections: A review, Pharmaceutics 14 (2) (2022), https://doi.org/10.3390/pharmaceutics14020427.

[51] X. Lv, L. Wang, A. Mei, Y. Xu, X. Ruan, W. Wang, J. Shao, D. Yang, X. Dong, Recent nanotechnologies to overcome the bacterial biofilm matrix barriers, Small 19 (6) (2023) 2206220, https://doi.org/10.1002/smll.202206220.

[52] Y. Zhu, S. Wu, Y. Sun, X. Zou, L. Zheng, S. Duan, J. Wang, B. Yu, R. Sui, F.J. Xu, Bacteria-targeting photodynamic nanoassemblies for efficient treatment of multidrug-resistant biofilm infected keratitis, Adv. Funct. Mater. 32 (14) (2022) 2111066, https://doi.org/10.1002/adfm.202111066.

[53] Y. Meng, L. Chen, Y. Chen, J. Shi, Z. Zhang, Y. Wang, F. Wu, X. Jiang, W. Yang, L. Zhang, C. Wang, X. Meng, Y. Wu, W. Bu, Reactive metal boride nanoparticles trap lipopolysaccharide and peptidoglycan for bacteria-infected wound healing, Nat. Commun. 13 (1) (2022), https://doi.org/10.1038/s41467-022-35050-6.

[54] M.G. Monaghan, R. Borah, C. Thomsen, S. Browne, Thou shall not heal: Overcoming the non-healing behaviour of diabetic foot ulcers by engineering the inflammatory microenvironment, Adv. Drug Deliv. Rev. (2023) 115120, https://doi.org/10.1016/j.addr.2023.115120.

[55] X. Wang, Q. Li, Y. Miao, X. Chen, X. Zhang, J. Shi, F. Liu, X. Wang, Z. Li, Y. Yang, X. Zhang, J. Wang, J. Duan, A 0d-2d heterojunction bismuth molybdate-anchored multifunctional hydrogel for highly efficient eradication of drug-resistant bacteria, ACS Nano 17 (16) (2023) 15568–15589, https://doi.org/10.1021/acsnano.3c02304.

[56] J. Liu, Y. Wang, W. Gao, M. Cao, H. Bian, S. Wang, L. Gui, C. Zhao, Y. Gu, Q. Zhong, Development of d–a–d-type nir-ii photothermal agents for synergistic eradication of multidrug-resistant bacteria and promoting diabetic wound healing, Adv. Funct. Mater. 35 (1) (2025) 2411986.

[57] M. Zhao, M. Kang, J. Wang, R. Yang, X. Zhong, Q. Xie, S. Zhou, Z. Zhang, J. Zheng, Y. Zhang, Stem cell-derived nanovesicles embedded in dual-layered hydrogel for programmed ros regulation and comprehensive tissue regeneration in burn wound healing, Adv. Mater. 36 (32) (2024) 2401369.

[58] L. Wang, L. Duan, G. Liu, J. Sun, M.A. Shahbazi, S.C. Kundu, R.L. Reis, B. Xiao, X. Yang, Bioinspired polyacrylic acid-based dressing: Wet adhesive, self-healing, and multi-biofunctional coacervate hydrogel accelerates wound healing, Adv. Sci. 10 (16) (2023) 2207352, https://doi.org/10.1002/advs.202207352.

[59] R. Yu, Y. Yang, J. He, M. Li, B. Guo, Novel supramolecular self-healing silk fibroin-based hydrogel via host–guest interaction as wound dressing to enhance wound healing, Chem. Eng. J. 417 (2021) 128278, https://doi.org/10.1016/j.cej.2020.128278.

[60] F. Caiado, T. Carvalho, F. Silva, C. Castro, N. Clode, J.F. Dye, S. Dias, The role of fibrin e on the modulation of endothelial progenitors adhesion, differentiation and angiogenic growth factor production and the promotion of wound healing, Biomaterials 32 (29) (2011) 7096–7105, https://doi.org/10.1016/j.biomaterials.2011.06.022.

[61] I. Bellos, V. Karageorgiou, V. Pergialiotis, D.N. Perrea, Acute kidney injury following the concurrent administration of antipseudomonal β-lactams and vancomycin: A network meta-analysis, Clin. Microbiol. Infect. 26 (6) (2020) 696–705, https://doi.org/10.1016/j.cmi.2020.03.019.